www.sciencemag.org/cgi/content/full/340/6130/337/DC1

Supplementary Materials for

# Multicompartment Mesoporous Silica Nanoparticles with Branched Shapes: An Epitaxial Growth Mechanism

Teeraporn Suteewong, Hiroaki Sai, Robert Hovden, David Muller, Michelle S. Bradbury, Sol M. Gruner, Ulrich Wiesner*

Corresponding author. E-mail: ubw1@cornell.edu

Published 19 April 2013, *Science* **340**, 337 (2013)
DOI: 10.1126/science.1231391

**This PDF file includes:**

## Materials and Methods

*Materials*

Hexadecyltrimethylammonium bromide (CTAB, approx. 99%), ethyl acetate (EtOAc, ACS grade), tetraethyl orthosilicate (TEOS, ≥99%, GC), (3-aminopropyl)triethoxysilane (APTES, > 95%), ammonium hydroxide ($NH_4OH$, 29%), acetic acid (glacial), hydrochloric acid (HCl, 36.5-38%), ethanol (absolute, anhydrous), ethanol amine (99%), iridium (III) chloride hydrate (99.9%) and deionized water (Milli-Q, 18.2 MΩ-cm) were used as obtained without further purification.

*Synthesis of multicompartment mesoporous silica nanoparticles (mc-MSNs)*

Multicompartment mesoporous silica nanoparticles (mc-MSNs) were prepared by increasing [EtOAc] in the synthesis of highly aminated cubic MSNs reported previously. (*19, 20*) The volumetric ratio in milliliters of chemicals used in the synthesis of cubic MSNs was 1 CTAB (aq):0.045 TEOS:0.055 APTES:0.54 $NH_4OH$:0.176 EtOAc:27.38 $H_2O$. For mc-MSNs, EtOAc volume per CTAB (aq) was varied from 0.264 for 137 mM to 0.880 for 457 mM. CTAB solution was gently stirred in a container to which $H_2O$, EtOAc, $NH_4OH$, and mixed silanes were added in this order. We note that after EtOAc addition, the mixture was left stirring for a few minutes to let the EtOAc dissolve before adding the rest of the reagents. Five minutes after silane addition was complete, $H_2O$ (7.98 v/v CTAB (aq)) was added and the mixture was left stirring for 24 hours. On completion of the reaction, samples were neutralized with 2 M HCl (aq), and the MSNs were cleaned of incorporated CTAB micelles with acetic acid as reported previously. The particles were redispersed in absolute ethanol or kept dry for storage to prevent further hydrolysis. In order to demonstrate the accessibility of higher-level particle architectures, syntheses were also performed as two-step processes. To that end to the reaction mixtures from [EtOAc] of 91 mM and 274 mM additional amounts of TEOS and APTES (either identical to or half of the initial amount) were added at 5 and 30 min aging time points. Results of the 91 mM EtOAc sample treated with half the initial amount of silanes (TEOS + APTES) at 30 min aging time is shown in Fig. 4M in the main text. Please note that through the amine in APTES the addition of monomers will lead to a slight increase of the solution pH.

In order to determine the surface amine content on the mc-MSN using elemental analysis by energy-dispersive x-ray spectroscopy (EDS), iridium (III) chloride hydrate was used as a contrasting agent according to previous literature (*28*).

*Measurement of solution pH*

The time dependent pH of the reactions was measured from model reactions in the absence of silanes (to protect the pH meter) or with equimolar amounts of ethanolamine to simulate the effect of the amine in APTES on pH. The reaction mixture pH was monitored with a VWR Model 8000 pH meter.

*Characterization*

Bright-field transmission electron microscopy (BF-TEM) images were obtained on a Tecnai T12 Spirit microscope, equipped with a $LaB_6$ source and a SIS Megaview III

CCD camera and running at an acceleration voltage of 120 kV. High-angle annular dark field scanning transmission electron microscopy (HAADF-STEM) images and EDS elemental maps were acquired on a Tecnai F20 microscope operating at an acceleration voltage of 200 kV and a camera length of 300 mm. Hanning-filtered Fast Fourier transform (FFT) images were calculated and analyzed in the Electron Direct Methods (EDM) software suite, version 3.0.

Small-angle x-ray scattering (SAXS) patterns of surfactant-extracted, dried MSN samples were obtained on a home-built rotating anode beamline as well as at the G1 station in Cornell High Energy Synchrotron Source (CHESS). (*19*, *20*) For the rotating anode setup, a flight path of 15 cm was used with the CuKα source, while a 40 cm flight path with 10 keV x-ray was used in CHESS G1. Two-dimensional patterns obtained on a phosphor-optical fiber coupled CCD were azimuthally integrated to generate the 1D SAXS patterns in the MATLAB software suite.

Nitrogen sorption experiments were performed on a Micromeritics ASAP2020 instrument. Around 10 mg of the samples were degassed at 110-120 °C under vacuum overnight prior to the measurements. Acquired isotherms were analyzed for pore size distribution using the non-local density functional theory (NLDFT) package using a cylindrical geometry and Tarazona's density functional model.

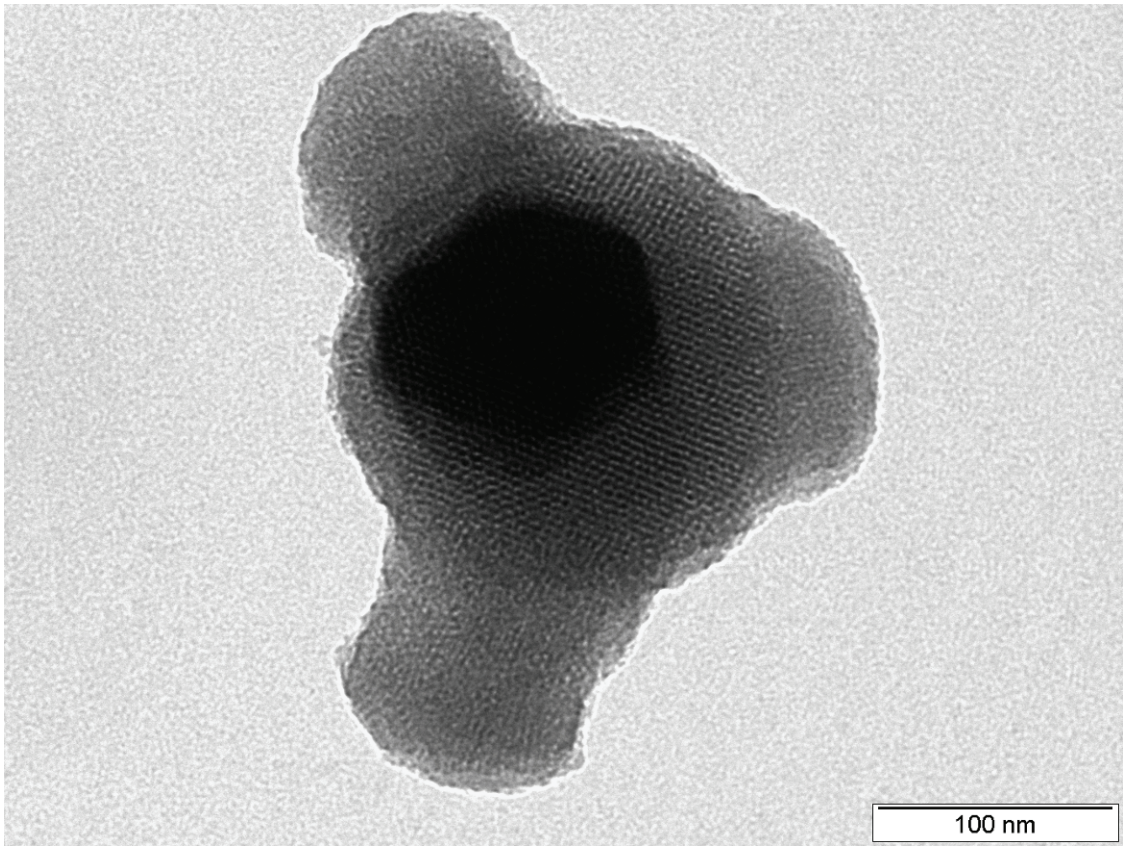


**Fig. S1.** TEM image of a mc-MSN showing one of the four branches (dark domain in the middle) growing in the same direction as the electron beam. Pore alignment geometry inside the hexagonal branch suggests that the external facets are parallel to the [10] direction of the hexagonal lattice, as shown in the model schematic in Fig. 1F in the main text.

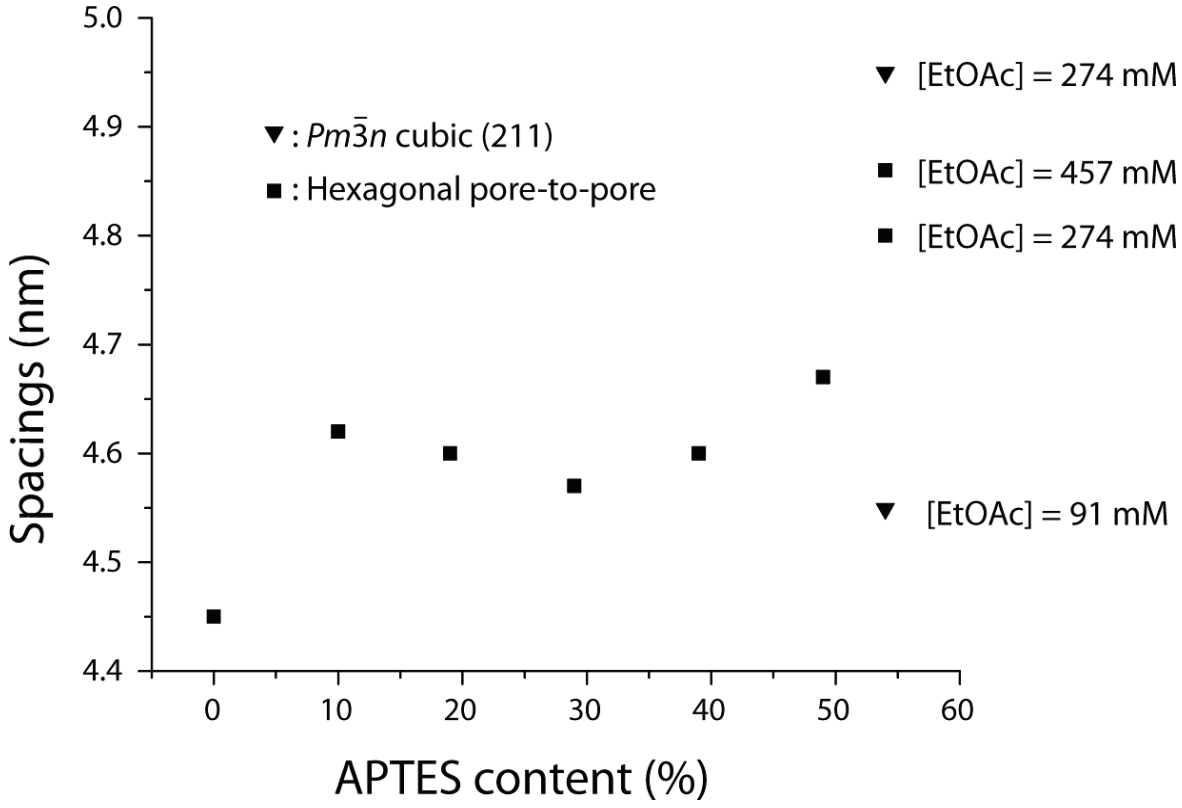


**Fig. S2.** Comparison of hexagonal pore-to-pore (squares) and cubic (211) (triangles) spacings in MSNs for varying amounts of APTES at a constant amount of EtOAc (91 mM), as well as for varying amounts of EtOAc at a constant amount of APTES (54 vol.%; 4 data points on the very right). Data points for 0-49 vol.% APTES in the synthesis feed are from a previous report. (*20*)

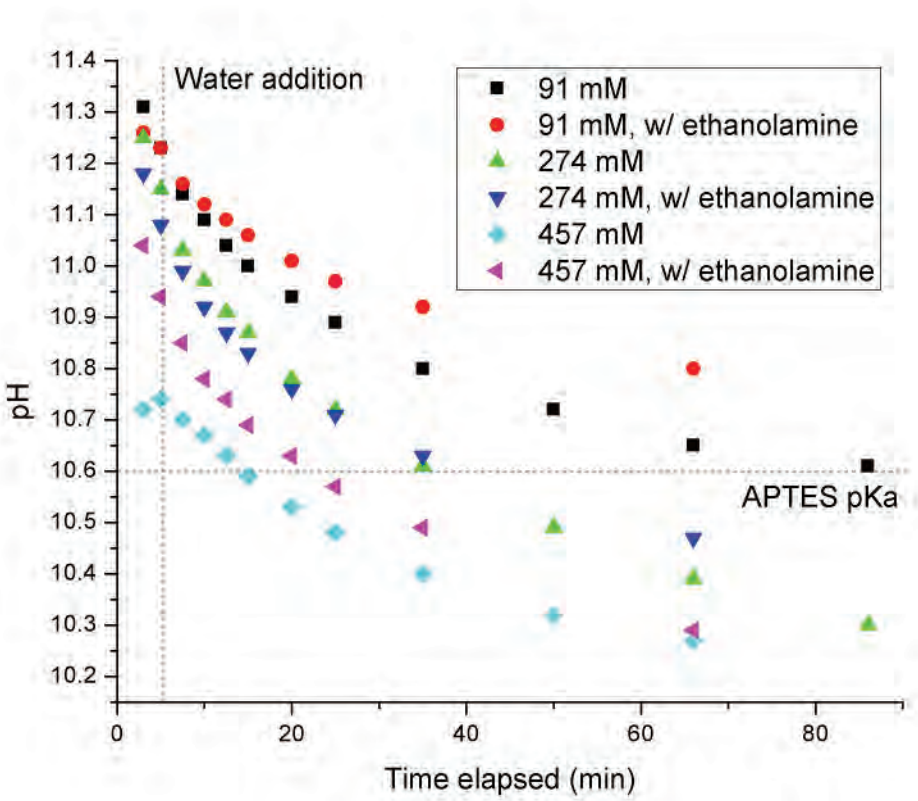


**Fig. S3**. pH evolution of reaction mixtures mimicking the condition for mc-MSN formation with varying [EtOAc]. Ammonium hydroxide solution and ethanolamine were added at 0 min, whereas the additional water was added at 5 min (perpendicular dashed line). pKa of APTES is shown as a horizontal dashed line for reference (*23*).

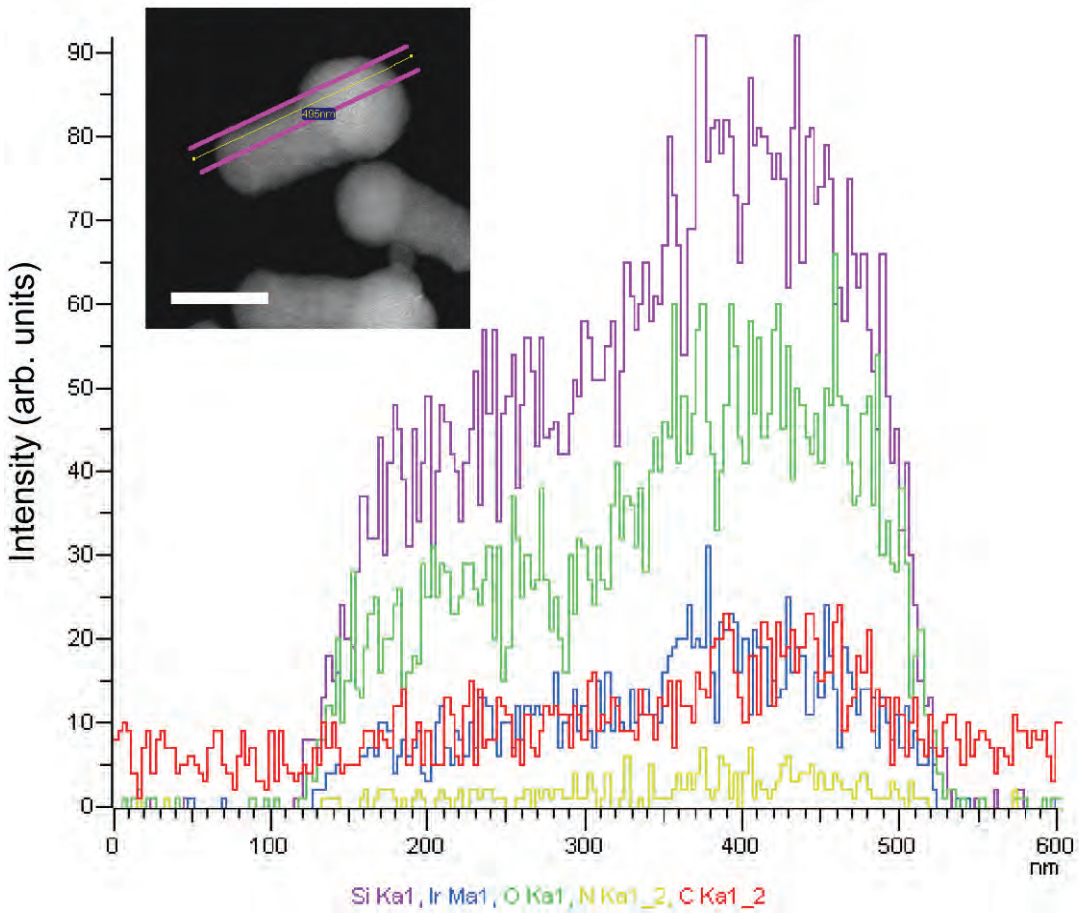


**Fig. S4**. EDS-derived elemental mapping profiles on a line slice of an iridium-stained mc-MSN. Inset shows the contour along which the spectra were taken. Scale bar is 200 nm. Note that the Si/Ir ratio difference between the branch and the core is insignificant, indicating that the amine content in the branch and core is similar.

**References**


1. T. Yanagisawa, T. Shimizu, K. Kuroda, C. Kato, The preparation of alkyltrimethylammonium-kanemite complexes and their conversion to microporous materials. *Bull. Chem. Soc. Jpn.* **63**, 988 (1990). doi:10.1246/bcsj.63.988

2. C. T. Kresge, M. E. Leonowicz, W. J. Roth, J. C. Vartuli, J. S. Beck, Ordered mesoporous molecular-sieves synthesized by a liquid-crystal template mechanism. *Nature* **359**, 710 (1992). doi:10.1038/359710a0

3. F. Hoffmann, M. Cornelius, J. Morell, M. Fröba, Silica-based mesoporous organic-inorganic hybrid materials. *Angew. Chem. Int. Ed.* **45**, 3216 (2006). doi:10.1002/anie.200503075 Medline

4. C. H. Xiao, N. Fujita, K. Miyasaka, Y. Sakamoto, O. Terasaki, Dodecagonal tiling in mesoporous silica. *Nature* **487**, 349 (2012). doi:10.1038/nature11230 Medline

5. M. Vallet-Regí, F. Balas, D. Arcos, Mesoporous materials for drug delivery. *Angew. Chem. Int. Ed.* **46**, 7548 (2007). doi:10.1002/anie.200604488 Medline

6. I. I. Slowing II, J. L. Vivero-Escoto, C. W. Wu, V. S. Lin, Mesoporous silica nanoparticles as controlled release drug delivery and gene transfection carriers. *Adv. Drug Deliv. Rev.* **60**, 1278 (2008). doi:10.1016/j.addr.2008.03.012 Medline

7. Z. B. Li, E. Kesselman, Y. Talmon, M. A. Hillmyer, T. P. Lodge, Multicompartment micelles from ABC miktoarm stars in water. *Science* **306**, 98 (2004). doi:10.1126/science.1103350 Medline

8. H. G. Cui, Z. Y. Chen, S. Zhong, K. L. Wooley, D. J. Pochan, Block copolymer assembly via kinetic control. *Science* **317**, 647 (2007). doi:10.1126/science.1141768 Medline

9. R. Chandrawati, M. P. van Koeverden, H. Lomas, F. Caruso, Multicompartment particle assemblies for bioinspired encapsulated reactions. *J. Phys. Chem. Lett.* **2**, 2639 (2011). doi:10.1021/jz200994n

10. L. Manna, D. J. Milliron, A. Meisel, E. C. Scher, A. P. Alivisatos, Controlled growth of tetrapod-branched inorganic nanocrystals. *Nat. Mater.* **2**, 382 (2003). doi:10.1038/nmat902 Medline

11. Y. Yin, A. P. Alivisatos, Colloidal nanocrystal synthesis and the organic-inorganic interface. *Nature* **437**, 664 (2005). doi:10.1038/nature04165 Medline

12. D. V. Talapin *et al*., Seeded growth of highly luminescent CdSe/CdS nanoheterostructures with rod and tetrapod morphologies. *Nano Lett.* **7**, 2951 (2007). doi:10.1021/nl072003g Medline

13. P. Srinivasu, S. Lim, Y. Kubota, T. Tatsumi, Synthesis of highly ordered mesoporous $P6_3/mmc$ and *P*6*mm* phases by adding alcohols to the system for the SBA-1 synthesis. *Catal. Today* **111**, 379 (2006). doi:10.1016/j.cattod.2005.10.049

14. L. Han, Y. Sakamoto, S. Che, O. Terasaki, Insight into the defects of cage-type silica mesoporous crystals with *Fd*3*m* symmetry: TEM observations and a new proposal of "polyhedron packing" for the crystals. *Chemistry* **15**, 2818 (2009). doi:10.1002/chem.200801688 Medline

15. R. Atluri, Z. Bacsik, N. Hedin, A. E. Garcia-Bennett, Structural variations in mesoporous materials with cubic symmetry. *Micropor. Mesopor. Mater.* **133**, 27 (2010). doi:10.1016/j.micromeso.2010.04.007

16. L. Han, K. Miyasaka, O. Terasaki, S. N. Che, Evolution of packing parameters in the structural changes of silica mesoporous crystals: Cage-type, 2D cylindrical, bicontinuous diamond and gyroid, and lamellar. *J. Am. Chem. Soc.* **133**, 11524 (2011). doi:10.1021/ja200683t Medline

17. S. N. Che, S. Kamiya, O. Terasaki, T. Tatsumi, The formation of cubic *Pm* macro 3*n* mesostructure by an epitaxial phase transformation from hexagonal p6mm mesophase. *J. Am. Chem. Soc.* **123**, 12089 (2001). doi:10.1021/ja0118237 Medline

18. S. Kamiya, H. Tanaka, S. Che, T. Tatsumi, O. Terasaki, Electron microscopic study of structural evolutions of silica mesoporous crystals: Crystal-growth and crystal-transformation from *P*6*mm* to with time. *Solid State Sci.* **5**, 197 (2003). doi:10.1016/S1293-2558(02)00094-8

19. T. Suteewong *et al*., Highly aminated mesoporous silica nanoparticles with cubic pore structure. *J. Am. Chem. Soc.* **133**, 172 (2011). doi:10.1021/ja1061664 Medline

20. T. Suteewong *et al*., Synthesis and formation mechanism of aminated mesoporous silica nanoparticles. *Chem. Mater.* **24**, 3895 (2012). doi:10.1021/cm301857e

21. See supplementary materials on *Science* Online.

22. T. Suteewong *et al*., Ordered mesoporous silica nanoparticles with and without embedded iron oxide nanoparticles: Structure evolution during synthesis. *J. Mater. Chem.* **20**, 7807 (2010). doi:10.1039/c0jm01002b

23. R. Atluri, Y. Sakamoto, A. E. Garcia-Bennett, Co-structure directing agent induced phase transformation of mesoporous materials. *Langmuir* **25**, 3189 (2009). doi:10.1021/la803727u Medline

24. G. Schulz-Ekloff, J. Rathousky, A. Zukal, Mesoporous silica with controlled porous structure and regular morphology. *Int. J. Inorg. Mater.* **1**, 97 (1999). doi:10.1016/S1463-0176(99)00015-0

25. L. W. Dittert, T. Higuchi, Rates of hydrolysis of carbamate and carbonate esters in alkaline solution. *J. Pharm. Sci.* **52**, 852 (1963). doi:10.1002/jps.2600520908 Medline

26. M. Ogura, H. Miyoshi, S. P. Naik, T. Okubo, Investigation on the drying induced phase transformation of mesoporous silica; a comprehensive understanding toward mesophase determination. *J. Am. Chem. Soc.* **126**, 10937 (2004). doi:10.1021/ja047785j Medline

27. Y. Wang *et al*., Colloids with valence and specific directional bonding. *Nature* **491**, 51 (2012). doi:10.1038/nature11564 Medline

28. J. Kecht, A. Schlossbauer, T. Bein, Selective functionalization of the outer and inner surfaces in mesoporous silica nanoparticles. *Chem. Mater.* **20**, 7207 (2008). doi:10.1021/cm801484r